Biomaterials Science

ROYAL SOCIETY OF CHEMISTRY

PAPER

View Article Online
View Journal | View Issue

Cite this: *Biomater. Sci.*, 2025, **13**, 6865

Fabrication of blood capillary microtissues without fibroblast support *via* growth factors and matrix stiffness modulation

He Li, [a] Fiona Louis [b] and Michiya Matsusaki *[a,b]

Received 27th June 2025,
Accepted 1st October 2025

DOI: 10.1039/d5bm00981b

rsc.li/biomaterials-science

The cells co-culture approach, involving endothelial cells and supporting stromal cells, such as fibroblasts, is commonly used for engineering microvascular networks. While this approach effectively promotes vascular morphogenesis through paracrine signaling and matrix remodeling, it often leads to excessive fibroblast proliferation. This uncontrolled growth can disrupt the structural organization of the developing vasculature, making it challenging to achieve reproducible and physiologically relevant microtissue architectures. In this work, we introduce an alternative monoculture method that uses only endothelial cells (HUVECs) in a fibrin gel matrix. To promote the formation of structured capillary-like networks without stromal support, we optimized vasculogenesis by supplementing exogenous vascular endothelial growth factor (VEGF), fine-tuning matrix stiffness, and applying it in a hypoxic environment (1% O_2). This approach was also applied to brain microvascular endothelial cells (BMEC) and liver sinusoidal endothelial cells (SEC). This innovation addresses the limitations of traditional methods, overcomes rapid matrix degradation caused by fibroblast-mediated remodeling, identifies ~2.56 kPa as the optimal stiffness for blood capillary growth, and demonstrates that capillary development is significantly enhanced at VEGF concentrations above 50 ng ml^{-1}.

1. Introduction

The construction of vascular networks represents a considerable challenge in the development of stable, large-scale tissues and organs *in vitro*. Tissue engineering continues to face major challenges in ensuring adequate oxygen and nutrient delivery over long distances, primarily due to limitations in passive diffusion. To address the requirements of the medical field, research on the construction of 3D capillary networks *in vitro* to form models similar to those in the living body has been actively promoted.

Most current strategies rely on co-culturing endothelial cells (ECs) with supporting stromal cells, such as fibroblasts, to facilitate capillary formation.[1,2] Fibroblasts secrete a variety of pro-angiogenic and stabilizing factors, including fibroblast growth factor (FGF), platelet-derived growth factor (PDGF), VEGF, transforming growth factor-β (TGF-β) and can adopt pericyte-like properties that promote endothelial tubulogenesis and vessel stabilization.[3,4] However, fibroblasts also exhibit aggressive proliferation and invasive behavior.[5] Through the secretion of matrix-remodeling enzymes such as matrix metalloproteinases (MMP-2 and MMP-9), they rapidly degrade protein-based hydrogels, often leading to premature matrix collapse.[6] In multi-lineage constructs, fibroblasts can overtake or disrupt the microenvironment of other cell types, interfering with tissue organization and compromising the structural and functional reproducibility of organoids.[7,8] These limitations highlight the need for alternative strategies that avoid the use of fibroblasts while maintaining physiological relevance.

Consequently, there is increasing interest in developing endothelial cell-only blood capillary models that utilize growth factors to mimic the supportive role of fibroblasts. Fujita *et al.*[9] first attempted to create capillary-like networks from ECs alone without supplemental growth factors. However, ECs cultured in isolation failed to self-organize into functional tubular structures, indicating the need for external cues. Campisi *et al.* used a microfluidic system combined with VEGF-A to support EC-only network formation. While vascular structures were formed, they exhibited excessive fusion and abnormally large diameters, approximately three times those observed in co-culture models, falling outside the physiological capillary range.[10] Li *et al.*[11] used 3D bioprinting to create rat EC-based networks under VEGF stimulation. The approach was technically complex and time-consuming because it required fine-tuning of bioink properties, repeated perform-

[a]*Department of Applied Chemistry, Graduate School of Engineering, Osaka University, 2-1 Yamadaoka, Suita, Osaka, 565-0871, Japan.*
E-mail: m-matsus@chem.eng.osaka-u.ac.jp; Tel: +81-6-6879-7357
[b]*Joint Research Laboratory (TOPPAN) for Advanced Cell Regulatory Chemistry, Osaka University, Suita, Osaka, Japan*

ance testing, and weekly transfer of hydrogel constructs during the 30-day culture period to maintain nutrient availability. These factors, together with the use of cross-species cells, limit its translational relevance to human physiology.

To overcome the major limitations of existing blood capillary models, we aimed to explore the synergistic regulation of both biochemical cues (*e.g.*, growth factors) and mechanical cues (*e.g.*, matrix stiffness) during angiogenesis to construct physiologically scaled microvascular networks composed solely of human ECs.[12] The VEGF family comprises several members, including VEGF-A, VEGF-B, VEGF-C, VEGF-D, placental growth factor (PlGF), and VEGF-E.[13] Among these, VEGF-A activates VEGFR1 and VEGFR2 to promote angiogenesis, increase vascular permeability, and stimulate endothelial cell migration. VEGF-C activates both VEGFR2 and VEGFR3 and plays a key role in sprouting and the formation of vascular networks during angiogenesis.[14] Hypoxia serves as a critical trigger for the hypoxia-inducible factor (HIF) pathway, which upregulates a wide array of angiogenic factors such as VEGF, PDGF-B, FGF, angiopoietin-1 (ANG-1), and angiopoietin-2 (ANG-2).[15] These molecules bind to corresponding receptors on endothelial cells, activating signaling pathways that drive proliferation, migration, and tube formation. Other molecules, such as MMPs and plasminogen activator inhibitor-1 (PAI-1), contribute to extracellular matrix (ECM) remodeling, further supporting vascular development.[4,6] Mechanical cues also critically influence angiogenesis. Endothelial cells can sense and respond to the stiffness of their microenvironment. In 3D tissue engineering, scaffolds with a tunable elastic modulus are essential for mimicking the biomechanical properties of native tissues. Softer matrices facilitate endothelial migration, leading to increased vessel length and branching. In contrast, stiffer matrices restrict migration and impair tube formation.[16]

In this study, we present a strategy for constructing capillary-scale vascular networks using only endothelial cells, without the need for fibroblast co-culture. By fine-tuning key parameters, such as cell density, oxygen levels, growth factor composition, and matrix stiffness, we successfully established self-organized vascular networks with morphological and functional features comparable to traditional co-culture systems. Importantly, this approach is also adaptable to other endothelial cell types, such as BMECs and SECs, making it broadly applicable across different tissue and organ systems. Comparative analysis revealed that the HUVEC-only model could recapitulate the vessel morphology of the NHDF and HUVEC co-culture group in terms of vascular density, vessel length, and vessel diameter, while maintaining spatial localization and functional organization of the cells along the vascular structures.

2. Materials and methods

2.1. Cell culture

Normal human dermal fibroblast cells (NHDF, CC-2509, Lonza, Basel, Switzerland) and cryopreserved human hepatic stellate cells (LX-2, SCC064, Sigma-Aldrich, USA) were cultured in Dulbecco's modified Eagle's medium (DMEM High-Glucose, 08458, Nacalai Tesque, Japan) with 10% fetal bovine serum (FBS, 35010163, Corning, USA) and 1% antibiotic (02892-54, Nacalai Tesque, Japan). Human umbilical vein endothelial cells (HUVEC, C25271, Lonza, Basel, Switzerland) were cultured in an endothelial growth medium (EGM-2MV, CC-3202, Lonza, Basel, Switzerland). Human brain microvascular endothelial cells/conditionally immortalized clone 18 (BMEC), HBVPC/ci37 human brain vascular pericytes conditionally immortalized clone 37 (HP) and HASTR/ci35 human astrocytes conditionally immortalized clone 35 (HA) were provided by Prof. Furihata from Chiba University (Chiba, Japan). BMEC were cultured in Vasculife VEGF-Mv Endothelial Complete Kit (LEC-LL-0005, Lifeline, USA) without the use of Gentamicin in the kit, and supplemented with 25 mL FBS and 1% antibiotic. HP were cultured in pericyte medium with complementary FBS and growth supplement (1201, ScienCell, USA). HA were cultured in DMEM culture medium with 5 ml N_2 supplement 100× (17502048, Gibco, USA), 5 ml antibiotics, and 50 ml FBS. BMEC, HP and HA were cultured on 100 mm diameter dishes precoated with collagen I (4020-010, Iwaki, Japan) in a 33 °C incubator with 5% CO_2 and cultured with 4 μg ml^{-1} Blasticidin S HCl (100011399, Gibco, USA) to maintain selective pressure during routine culture. Human sinusoidal endothelial cells (SECs) (30047, ScienCell, USA) were transduced with the immortalizing genes GFP-SV40T and hTERT to establish the GFP-SEC cell line used in this study. GFP-SEC were cultured in the endothelial cell medium (1001, ScienCell, USA). For all experiments, cells of all types were used at passages 4–7.

2.2. Fabrication of 3D HUVEC blood capillary microtissue models

Three-dimensional blood capillary microtissues were fabricated following previously reported methods with minor modifications.[17] Briefly, thrombin (T4648, Sigma-Aldrich, USA) was dissolved in DMEM containing 10% FBS at a concentration of 7.5 U mL^{-1}, sterilized using a 0.22 μm filter, and mixed with cells to form Solution 1. For Solution 1, 2×10^4 NHDFs and 1×10^4 HUVECs, or only 1×10^4, 2×10^4, or 3×10^4 HUVECs were used. VEGF-A (225-02471, Fujifilm, Japan) and VEGF-C (9199-VC-025/CF, R&D Systems, USA) were diluted in DMEM without FBS to final concentrations of 25, 50, and 100 ng mL^{-1}. Fibrinogen (F8630, Sigma-Aldrich, USA) was dissolved in DMEM without FBS at concentrations of 7.5, 15, 30, 60, 125, and 250 mg mL^{-1} to prepare Solution 2.

For tissue construction, a 10 μL mixture was prepared as follows: **HUVEC-only tissues**: 4 μL of Solution 1 + 1 μL VEGF-A + 1 μL VEGF-C + 4 μL of Solution 2. **NHDF and HUVEC co-cultured tissues**: 4 μL of Solution 1 + 2 μL DMEM (without FBS) + 4 μL of Solution 2. The mixtures were seeded into 48-well plates (one droplet per well) and incubated at 37 °C for 30 min to gelate. Following gelation, 1 mL of EGM-2 culture medium, supplemented with VEGF-A and/or VEGF-C at 0, 25, 50, or 100 ng mL^{-1}, was added to each well. Tissues were cultured under

hypoxic (1% O_2) or normoxic (21% O_2) conditions for 7 days, with half of the culture medium replaced every 2–3 days.

2.3. Fabrication of BMEC-only and BMEC-HP-HA co-cultured vascular microtissues

BMEC-only microtissues were prepared using the same method as for HUVEC-only microtissues, with adjustments for cell type and culture conditions. BMECs were seeded at 1×10^4, 2×10^4, or 3×10^4 cells per droplet, and fibrinogen was used at final concentrations of 3, 6, 12, or 24 mg mL^{-1} to explore different scaffold mechanical properties. After gelation, 1 mL of Vasculife culture medium supplemented with 50 ng mL^{-1} VEGF-A and VEGF-C was added, and the medium was half refreshed every 2–3 days. BMEC (3×10^4), HP (1.5×10^4), and HA (6×10^4) co-cultured microtissues were constructed as a positive control to compare the vascularization capacity of co-cultured *versus* BMEC-only tissues under both normoxic and hypoxic conditions.

2.4. Immunostaining and fluorescence imaging

To better observe the microvascular network, the nuclei were detected by Hoechst 33342 (H3570, Thermo Fisher, USA), and HUVECs or BMEC or SEC were immunostained by anti-CD31 (M082301-2, DAKO, Denmark). After 7 days of culture, the microtissues were fixed in 4% paraformaldehyde (PFA, 30525-89-4, Wako, Japan) for 15 min at room temperature. Thereafter, the tissues were rinsed 3 times with PBS. Subsequently, the tissue permeabilization was performed with 0.02% Triton X-100 (T8787, Sigma-Aldrich, USA) in PBS for 15 min, followed by blocking with 1% bovine serum albumin (BSA, A3294, Sigma-Aldrich, USA) in PBS for 1 h. After washing 3 times with PBS, tissues were incubated with primary antibodies (anti-CD31 antibody, diluted at 1 : 50 in 1% BSA in PBS) overnight at 4 °C. After washing the tissues 3 times with PBS, the secondary antibodies (goat-anti mouse, Alexa Fluor 647, A21235, Thermo Fisher, co-stained with Hoechst 33342, 1 : 100 dilution in 1% BSA in PBS) were incubated for 2 h in a dark environment at room temperature. The tissues were then treated for clearance with Rapiclear 1.52 (RC152001, Sunjin lab, China) for 2 h, a process that rendered the hydrogel transparent and facilitated the observation of the vascular structures with greater clarity. The 3D tissue was finally observed using a confocal laser scanning microscope (CLSM) (Confocal Quantitative Image Cytometer CQ1, Yokogawa, Japan). In three independent experiments, each included 16 high-resolution confocal images, with each image acquired as a z-stack composed of 9 to 11 slices at 5 μm step size.

2.5. Blood capillary image analysis

The microvascular vessel density, total vessel length, junction density, and lacunarity were analyzed using AngioTool software (Version 0.6 a, National Cancer Institute, USA).[18] Thresholds and small particle removal parameters were manually adjusted to ensure that all tubular structures were accurately selected by AngioTool. Blood capillary-related metrics were then automatically quantified based on the processed images. The AngioTool analysis workflow and representative images of the results are shown in the SI, Fig. S15. The average vessel diameter was analyzed using ImageJ software (Fiji, version 1.54p, National Institutes of Health, USA). For every sample, 50 times measurements were taken manually.

2.6. Fibrin gel construction and elastic modulus measurement

Fibrinogen was dissolved in PBS at 6, 12, 24, 48, 100, 200 mg ml^{-1}. Thrombin was dissolved in PBS at 6 U ml^{-1}. Five individual 100 μL of the mixed solution (50 μL fibrinogen with different concentrations and 50 μL thrombin) was then quickly seeded into a 60 mm dish. After that, the fibrin drops were incubated in a 37 °C incubator for gelation. After 1 h, the gels were meticulously retrieved using tweezers and transferred to a clean compression test bench, taking care to avoid any damage to the hydrogel.

Compression tests were conducted at room temperature using the EZ-TEST instrument (AGS-X, Shimadzu, Japan) with a 1 N load cell at a compression strain rate of 20.0 μm min^{-1}. Before testing, the diameter and height of each gel sample were measured using a Vernier caliper. The deformation of each sample was recorded and the stress–strain curve was obtained. The elastic modulus was selected within the range of 10% to 20% of the sample thickness, and it was calculated automatically by TRAPEZIUM LITE X (Version 1.5.8, Shimadzu, Japan).

2.7. Histology

The 10 μL microtissue samples were fixed in 4% PFA overnight at 4 °C, and sent to the Applied Medical Research company (Osaka, Japan) for paraffin wax embedding, hematoxylin eosin (HE) staining and CD31 (ab182981, Abcam, UK) staining. During paraffin embedding and sectioning, a longitudinal cut was made through the central region of the hydrogel for hydrogel size analysis. The histology was observed using an FL Evos Auto microscope (Thermo Fisher, USA) at 10× and 40× magnification.

2.8. PCR analysis

RNA extraction. RNA extraction was performed on two types of 3D blood capillary microtissue model ($n = 3$): For HUVEC-only tissue: 2×10^4 HUVEC was seeded in the fibrin gel where the final concentration of fibrinogen was 12 mg ml^{-1}, and 3 U ml^{-1} thrombin and they were then cultured in a 1% O_2 incubator for 7 days ("HUVEC-only" group). For NHDF and HUVEC co-culturing tissue, 2×10^4 NHDF and 1×10^4 HUVEC were seeded in the same fibrin gel as the HUVEC-only tissue, and incubated in 21% O_2 for 7 days ("Co-culture" group). All the samples were rinsed once with PBS and then lysis was performed using the PicoPure™ RNA Isolation Kit (KIT0204, Thermo Fisher, USA) until the RNA was extracted. Extracted RNA was quantified using a NanodropTM N1000 device (Thermo Fisher, USA).

cDNA synthesis and qRT-PCR. For RT-qPCR, the RNA samples were first submitted to reverse transcription into

cDNA using iScript cDNA synthesis kit (1708890, Bio-Rad, USA), before being amplified using Taqman probes and reagents (Taqman Fast Advanced Mix, Taqman gene expression assays (FAM): PPIA (Assay ID: Hs04194521_s1), CD34 (Assay ID: Hs02576480_m1), ICAM1 (Assay ID: Hs00959180_g1), FLT1 (Assay ID: Hs01052961_m1), KDR (Assay ID: Hs00911700_m1), Thermo Fisher, USA). The cDNA synthesis and RT-qPCR reactions were conducted using the StepOnePlus Real-Time PCR System (Thermo Fisher, USA) and the gene expression was normalized by PPIA as the housekeeping gene. Results were moreover standardized by CD31 expression to highlight the gene expression of the endothelial cells.

2.9. Statistical analysis

All data are expressed as the mean ± SD. For multifactorial data, an ANOVA analysis with a Tukey's test was used. For other between-group analysis statistics, a one-way t-test was used. Specific experimental analyses are described in the figure notes. *P*-Values are indicated directly on the graph to denote statistical significance.

3. Results

3.1. Optimization of HUVEC seeding density and oxygen conditions for capillary network formation

Four experimental groups were established as described in the Methods, with different cell types and HUVEC seeding densities: (i) NHDF and HUVEC, (ii) HUVEC 1×10^4, (iii) HUVEC 2×10^4, and (iv) HUVEC 3×10^4 (Fig. 1a). In each group, blood capillary networks were formed under both normoxic and hypoxic conditions (Fig. 1b and c). To determine the geometrical changes in the models, vessel density, junction density, total vessel length, lacunarity, and average vessel diameter were each quantified (Fig. 1d–h). Under hypoxia, the vessel density in the NHDF and HUVEC co-culture group (26.8 ± 2.2%) (Fig. 1c(i)) was significantly reduced compared to normoxia (44.1 ± 6.8%) (Fig. 1b(i) and d). In contrast, vessel density, junction density, and total vessel length showed no significant differences between normoxia and hypoxia among all three HUVEC-only groups at their respective cell seeding densities (Fig. 1d–g). Notably, under normoxia, the average vessel diameters in the HUVEC-only groups showed a clear cell number dependent increase, with average diameters of 24.7 ± 3.3 μm, 49.4 ± 3.6 μm, and 72.9 ± 12.0 μm for the HUVEC 1×10^4, 2×10^4, and 3×10^4 groups, respectively (Fig. 1h). These values were significantly larger than the diameter observed in the positive control group (NHDF + HUVEC) under normoxia (19.9 ± 1.2 μm). However, in hypoxic conditions, all groups showed average diameters below 30 μm (Fig. 1h), and no significant differences were observed between the 2×10^4 and 3×10^4 HUVEC groups across any of the five vascular parameters.

In summary, these results suggest that hypoxia limited the vessel diameter formed by HUVEC-only to within 30 μm, closely resembling the size and morphology of capillaries in the co-culture model, which is widely recognized for better physiological relevance.[10] Among the HUVEC-only groups under hypoxia, both the 2×10^4 and 3×10^4 cell density groups produced vascular networks with comparable density, junction complexity, total length, and lacunarity to those of the NHDF + HUVEC co-culture model. However, sprouting beyond the hydrogel boundary was occasionally observed in the 3×10^4 group, indicating reduced spatial control. Based on these findings, we selected the HUVEC 2×10^4 group under hypoxic conditions for use in subsequent experiments.

3.2. Influence of growth factor supplementation on capillary morphogenesis

To further investigate the role of growth factors in blood capillary formation, a HUVEC-only model was established and treated with 0–100 ng mL^{-1} of VEGF-A and (or) VEGF-C, both within the hydrogel and supplemented in the culture medium (Fig. 2a–c).

We first examined the effects of different VEGF types. In the absence of VEGF, minimal capillary formation was observed, with a vessel density of 29.8 ± 0.8% (Fig. 2d), and ECs predominantly formed aggregates at the periphery of the tissue model (Fig. 2c(i)). The addition of either VEGF-A or VEGF-C significantly enhanced vessel density to 40.5 ± 1.5% and 40.6 ± 3.5%, respectively, and promoted outward extension of vascular structures (Fig. 2b–d). Notably, the average vessel diameter in the VEGF-C-only group was significantly smaller (15.2 ± 2.0 μm) than in the VEGF-A or VEGF-A + C groups (>25 μm) (Fig. 2e). The combination of VEGF-A and VEGF-C further increased vessel density to 48.6%, accompanied by more complex networks with extensive branching and an elevated junction density of 57.2% (Fig. 2f). The average vessel diameter in this group (28.5 ± 0.8 μm) was comparable to that in the VEGF-A-only group (27.0 ± 0.4 μm) (Fig. 2e).

Next, we assessed the impact of VEGF-A and VEGF-C at varying concentrations (0, 25, 50, and 100 ng mL^{-1}). Total vessel lengths in these groups were 89.7 μm, 166.4 μm, 193.1 μm, and 175.0 μm, respectively, with the difference between 50 and 100 ng mL^{-1} not being statistically significant (Fig. 2g). Vessel length, density, and complexity increased in a dose-dependent manner up to 50 ng mL^{-1}, beyond which the effect plateaued. In contrast, average vessel diameter remained consistent across concentrations, ranging between 26 and 28 μm. Based on these findings, the optimal condition for capillary induction was determined to be 50 ng mL^{-1} of both VEGF-A and VEGF-C.

3.3. Impact of scaffold mechanical properties on blood capillary development

We investigated the relationship between the elastic modulus of fibrin hydrogels and the concentrations of fibrinogen and thrombin. Hydrogels were first formed using fibrinogen at 3 or 6 mg mL^{-1} and thrombin at 3 or 6 U mL^{-1}, and their stiffness was measured by compression testing. At a fixed thrombin concentration, the gel formed with 12 mg mL^{-1} fibrinogen exhibited an elastic modulus two times higher than that of the

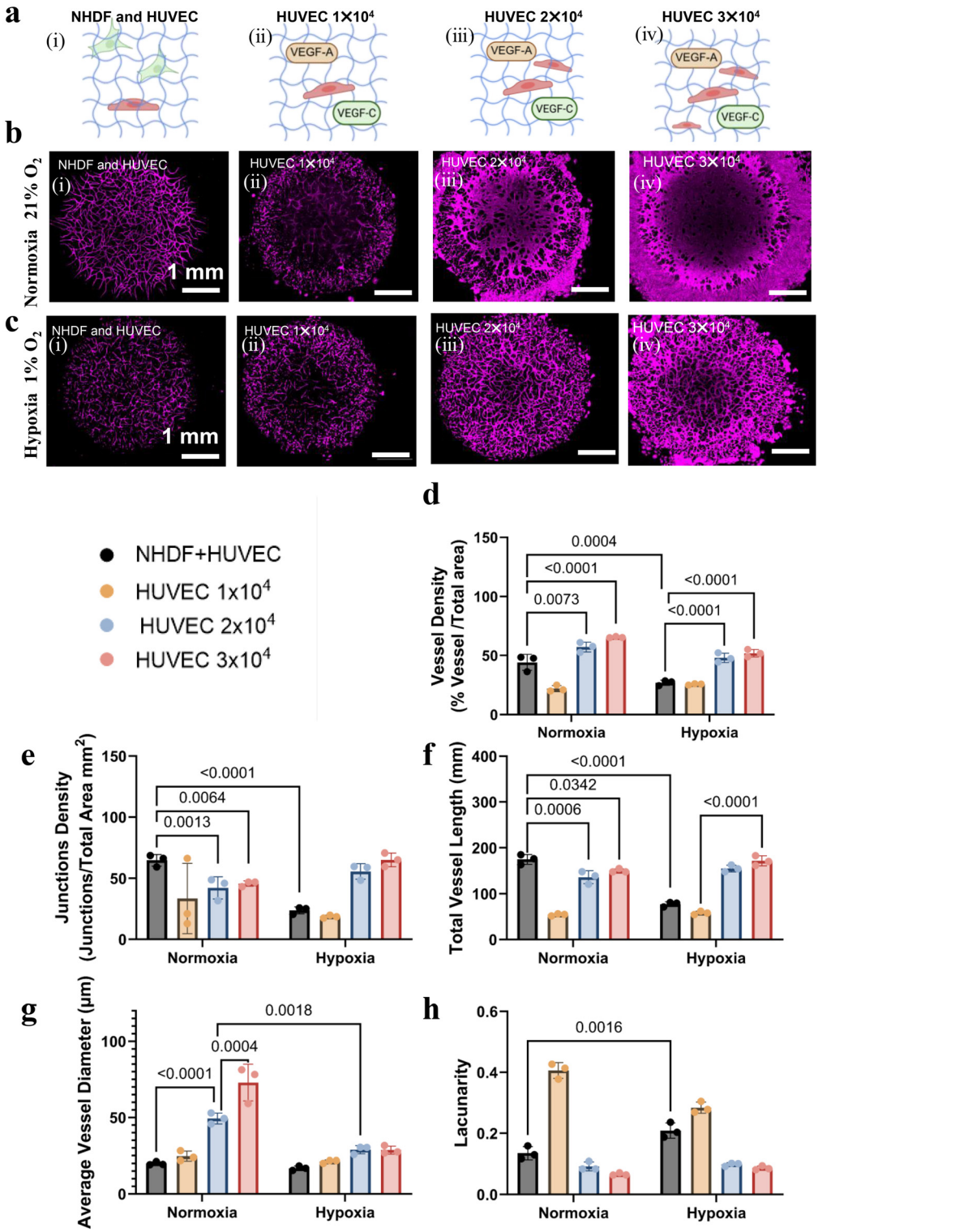

Fig. 1 Optimization of HUVEC seeding density and oxygen conditions for capillary network formation. (a) Schematic representation. (b and c) Observation of blood capillary by CD31 immunostaining under CLSM. (b and c, (i)) NHDF and HUVEC co-culture (NHDF 2×10^4 and HUVEC 1×10^4) as a control to compare with HUVEC-only microtissue. The HUVEC numbers are (b and c, (ii)) 1×10^4, (b and c, (iii)) 2×10^4, and (b and c, (iv)) 3×10^4 for HUVEC-only microtissue. Culturing all the microtissues in both normoxia (21% O_2) and hypoxia (1% O_2). All HUVEC-only groups were supplemented with 50 ng ml^{-1} VEGF-A and 50 ng ml^{-1} VEGF-C. Scale bar = 1 mm. (d–h) The vessel density, junction density, total vessel length, average vessel diameter, and lacunarity in the whole microtissue of the 3D capillary structure were calculated by AngioTool (n = 3). Statistical analysis was performed using two-way ANOVA followed by Tukey's test. P-Values are indicated directly on the graph to denote statistical significance.

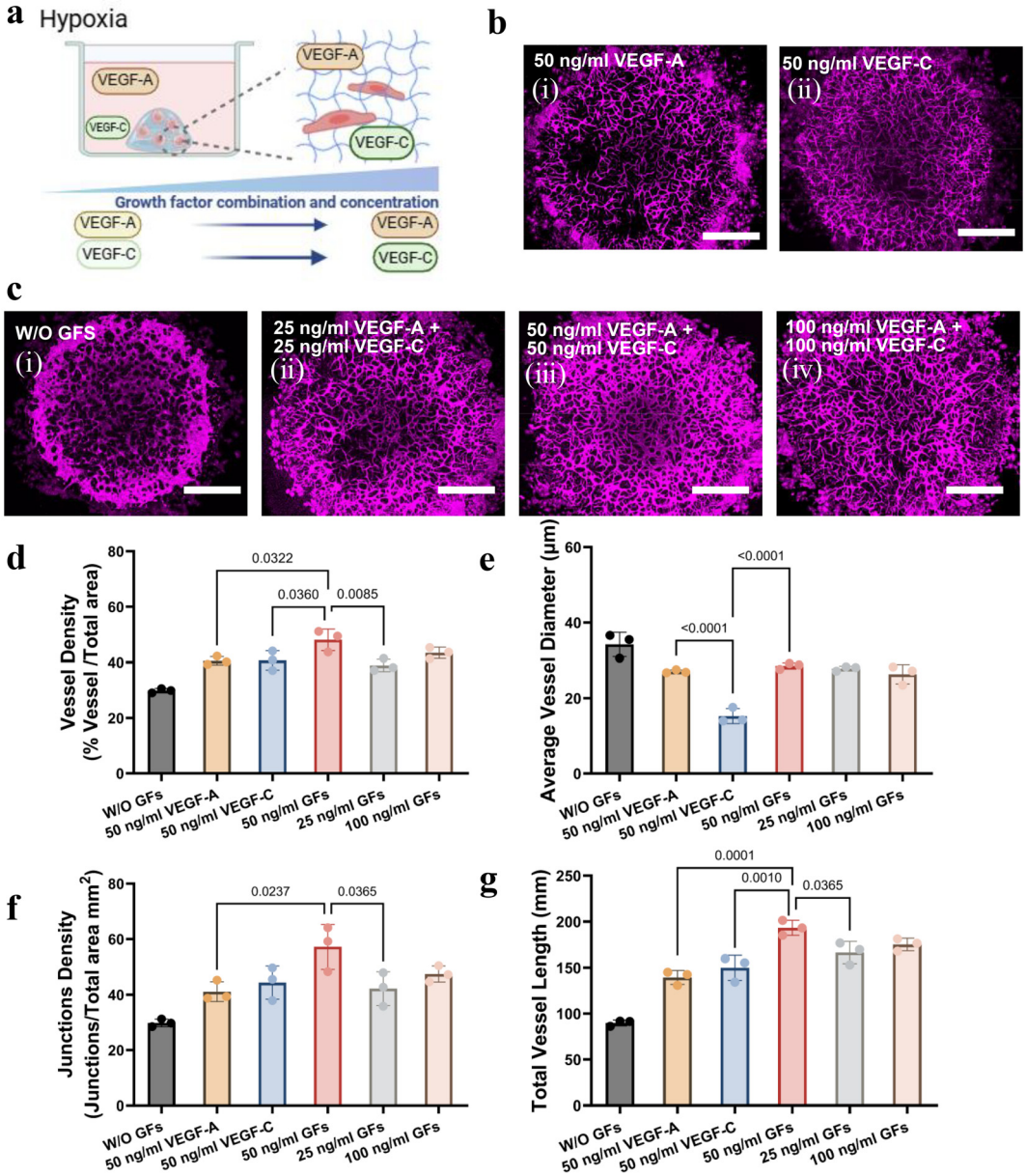

Fig. 2 Influence of growth factor supplementation on capillary morphogenesis. (a) Schematic representation. (b and c) Observation of blood capillary by CD31 immunostaining under CLSM. Culture HUVEC-only tissue (2×10^4 HUVEC) in hypoxia (1% O_2) with (b(i)) 50 ng ml^{-1} VEGF-A, (b(ii)) 50 ng ml^{-1} VEGF-C, (c(i)) without growth factors (W/O GFs), (c(ii)) 25 ng ml^{-1} VEGF-A and 25 ng ml^{-1} VEGF-C combination (25 ng ml^{-1} GFs), (c(iii)) 50 ng ml^{-1} VEGF-A and 50 ng ml^{-1} VEGF-C combination (50 ng ml^{-1} GFs), and (c(iv)) 100 ng ml^{-1} VEGF-A and 100 ng ml^{-1} VEGF-C combination (100 ng ml^{-1} GFs). Scale bar = 1 mm. (d–g) The vessel density, average vessel diameter, junction density, total vessel length in the whole microtissue of the 3D capillary structure were calculated by AngioTool (n = 3). Data are presented as means ± S.D. Statistical analysis was performed using one-way ANOVA followed by Tukey's test. P-Values indicate significance.

gel formed with 6 mg mL^{-1} fibrinogen (Fig. S2). However, variations in thrombin concentration did not result in statistically significant differences in gel stiffness. These findings indicate that the increase in elastic modulus was primarily driven by fibrinogen concentration rather than thrombin. To systematically evaluate the impact of fibrinogen concentration, we prepared hydrogels with final fibrinogen concentrations of 3, 6, 12, 24, 50, and 100 mg mL^{-1}, using 3 U mL^{-1} thrombin for polymerization. The resulting elastic modulus values ranged from 0.45 to 14.53 kPa, showing a positive correlation between scaffold stiffness and fibrinogen concentration (Fig. 3a).

VEGF concentration is a critical determinant of both the onset and rate of vascular growth.[19] To minimize potential confounding, we maintained constant levels of 50 ng ml^{-1} VEGF-A and 50 ng ml^{-1} VEGF-C in all experiments assessing the impact of matrix stiffness on capillary network formation using two types of vascular models, HUVEC-only groups and NHDF + HUVEC co-cultured groups (Fig. 3b and c). We quanti-

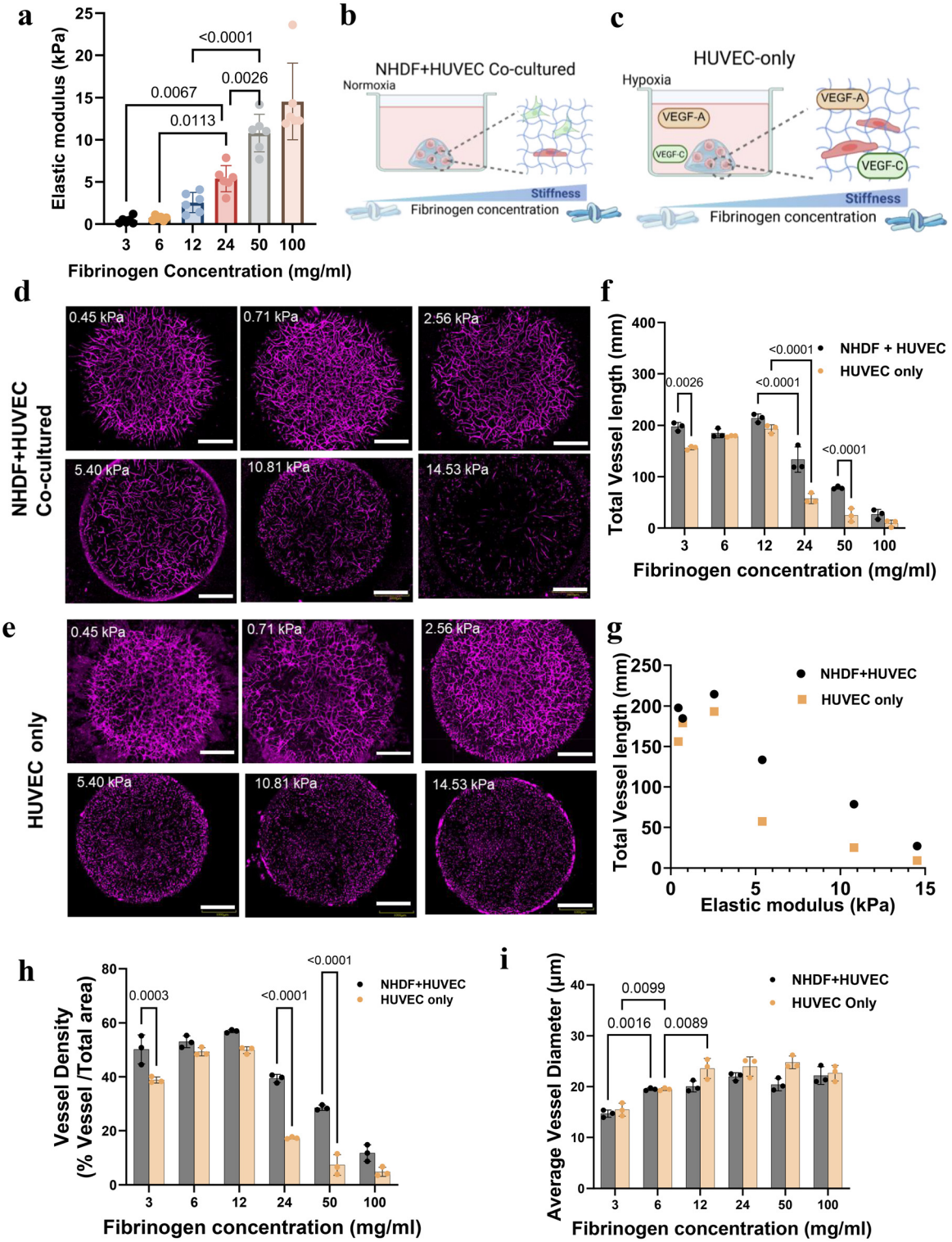

Fig. 3 Impact of scaffold mechanical properties on blood capillary development. (a) Compression test to measure the elastic modulus of the fibrin scaffold (n = 5). The elastic modulus is affected by fibrinogen concentration. (b and c) Schematic representation. (d) Observation of blood capillary by CD31 immunostaining under CLSM. Culture NHDF and HUVEC co-culture tissue (2×10^4 NHDF and 1×10^4 HUVEC) in normoxia (21% O_2) on different stiffness matrices. (e) Culture HUVEC-only tissue (2×10^4 HUVEC) in hypoxia (1% O_2) on different stiffness matrices. Scale bar = 1 mm. (f and h–i) The total vessel length, vessel density, and average vessel diameter in the whole microtissue of the 3D capillary structure were calculated by AngioTool (n = 3). (g) The relationship between matrix elastic modulus and blood capillary total vessel length in microtissue. The blood capillary length was dependent on the elastic modulus of the scaffold. Statistical analysis was performed using two-way ANOVA followed by Tukey's test. P-Values indicate significance.

fied the total vessel length in different scaffold stiffnesses and analyzed their relationship. A clear correlation was observed between total capillary length and hydrogel stiffness in both models (Fig. 3d–g). The greatest total vessel lengths were observed in the 2.56 kPa scaffolds, 193.1 mm in the HUVEC-only model and 214.2 mm in the co-culture model. In contrast, stiffer matrices (5.4–14.53 kPa) showed twice reduced vessel density, with total lengths ranging from 60 mm down to 9 mm (Fig. 3f).

Interestingly, in the softest scaffolds (0.45 kPa), both models generated narrow, filamentous capillary structures with average diameters less than 15.5 μm. In contrast, capillaries formed in stiffer matrices had an enlarged diameter, ranging from 20 to 25 μm (Fig. 3d, e, i and S4). Notably, the HUVEC-only tissues were more sensitive to matrix stiffness variations than co-cultured tissues (Fig. 3e and S4). In low-stiffness hydrogels, cells tended to migrate and grow toward the outer regions of the gel (Fig. 3d and e).[20]

3.4. Optimization of culture time for HUVEC-only capillary networks

Based on the optimized conditions identified above, HUVEC-only tissues were cultured for varying culture times to assess vascular development over time (Fig. 4a). HUVECs elongated after 1 day, but no capillary structures had formed. Capillary-like networks began to appear at days 3 and 5, with vessel densities of 11.7% and 29.0%, respectively (Fig. 4b and c). After 7 days, the vascular network formed into a highly interconnected structure, reaching a peak vessel density of 44.8% and a maximum junction density of 48.6% (Fig. 4c and d).

At later time points (days 10 and 14), slight degradation of the capillary structures was observed, with vessel densities declining to 42.7% and 37.7%, respectively, though these changes were not statistically significant (Fig. 4c). Notably, CD31 staining revealed HUVECs had slightly migrated beyond the hydrogel boundary at both time points, indicating partial outgrowth of HUVECs from the hydrogel matrix (Fig. 4b). Other vascular parameters, including total vessel length, junction density, and lacunarity, followed a similar temporal trend (Fig. 4d–f). In contrast, the average vessel diameter increased between days 3 and 5 of culture, and remained stable from day 5 to day 14 (Fig. 4g). Based on these characteristics, a 7-day culture time was selected as the optimal time point for subsequent experiments.

3.5. Cells and vasculature localization and gene expression related to blood capillary

The two models (i) NHDF + HUVEC co-culture and (ii) HUVEC-only monoculture were established based on previously optimized conditions (Fig. 5a). CD31 (magenta) marked the location of blood vessels, while Hoechst (blue) stained cell nuclei. In the monoculture group, cells were found confined within the hydrogel and co-localized with the capillary structures. In contrast, in the co-culture group, numerous cells were observed outside the hydrogel boundary (Fig. 5b).

Histological analyses further revealed differences in cell distribution and vascular morphology between the two models. Both HE staining (Fig. S5) and CD31 immunohistochemistry (IHC) confirmed capillary formation in each group (Fig. 5c). A distinct surface cell layer was observed in the co-culture group (Fig. 5c, black arrow, Fig. S6), but not in the HUVEC-only model. This observation aligns with the outgrowth of cells beyond the hydrogel seen in the co-culture group in the immunofluorescence image (Fig. 5b). Longitudinal sections from the center of the hydrogels were analyzed to evaluate morphological changes over time relative to day 0 (Fig. S5). In the co-culture model, tissue height decreased by 50.9%, while cell area/tissue diameter increased by 40.6%, and the area decreased by 42.2%, indicating substantial lateral tissue expansion and fibrin degradation. In contrast, the HUVEC-only model showed a smaller change, with height decreasing only by 12.2% and diameter increasing by 10.6%, and the area remained essentially unchanged, suggesting markedly better VEGF concentration is a critical determinant of both the onset and rate of vascular growth Quantification of CD31 immunostaining showed comparable expression levels between the two models, indicating similar levels of endothelial structure formation despite morphological differences (Fig. 5f). From the zoomed-in images, the lumen structures can be clearly observed in both vascular models (Fig. S8). To assess whether the engineered HUVEC-only microvascular model could serve as a physiologically relevant substitute for the traditional co-culture system, we compared gene expression *via* RT-PCR after 7 days of culture. Total RNA was extracted from optimized tissue constructs (Fig. 5a). RT-PCR analysis was conducted considering gene markers of vascular related protein-like platelet endothelial cell adhesion molecule (CD31), human hematopoietic progenitor cell antigen (CD34), intercellular adhesion molecule 1 (ICAM1) and growth factor receptors such as VEGFR-1 (FLT1) and VEGFR-2 (KDR). Vessel angiogenesis and maturation were investigated in terms of the expression of several markers and proteins, in the case of HUVEC-only conditions and were compared to the co-cultured condition. The mRNA expression of each gene was measured relative to the expression of CD31 and PPIA (housekeeping gene). In the monoculture condition, all tested genes, CD34, FLT1, KDR, and ICAM1, were expressed at lower levels compared to the co-culture group, with significant differences observed in particular in FLT1 and ICAM1 expressions (Fig. 5g).

3.6. Construction of monocultured blood capillary networks using other endothelial cell lines

To evaluate the broad applicability of our endothelial cell-only model for capillary network formation, we extended our investigation to include two additional endothelial cell types, BMECs and SECs, which are representative of the brain and liver microvascular systems, respectively.

Given the distinct characteristics of these cell types, we first optimized the experimental conditions by varying both cell seeding densities (0.5×10^4–3×10^4 cells) and matrix stiffness (0.45 kPa–5.4 kPa) in fibrin hydrogels. In BMEC-only cultures,

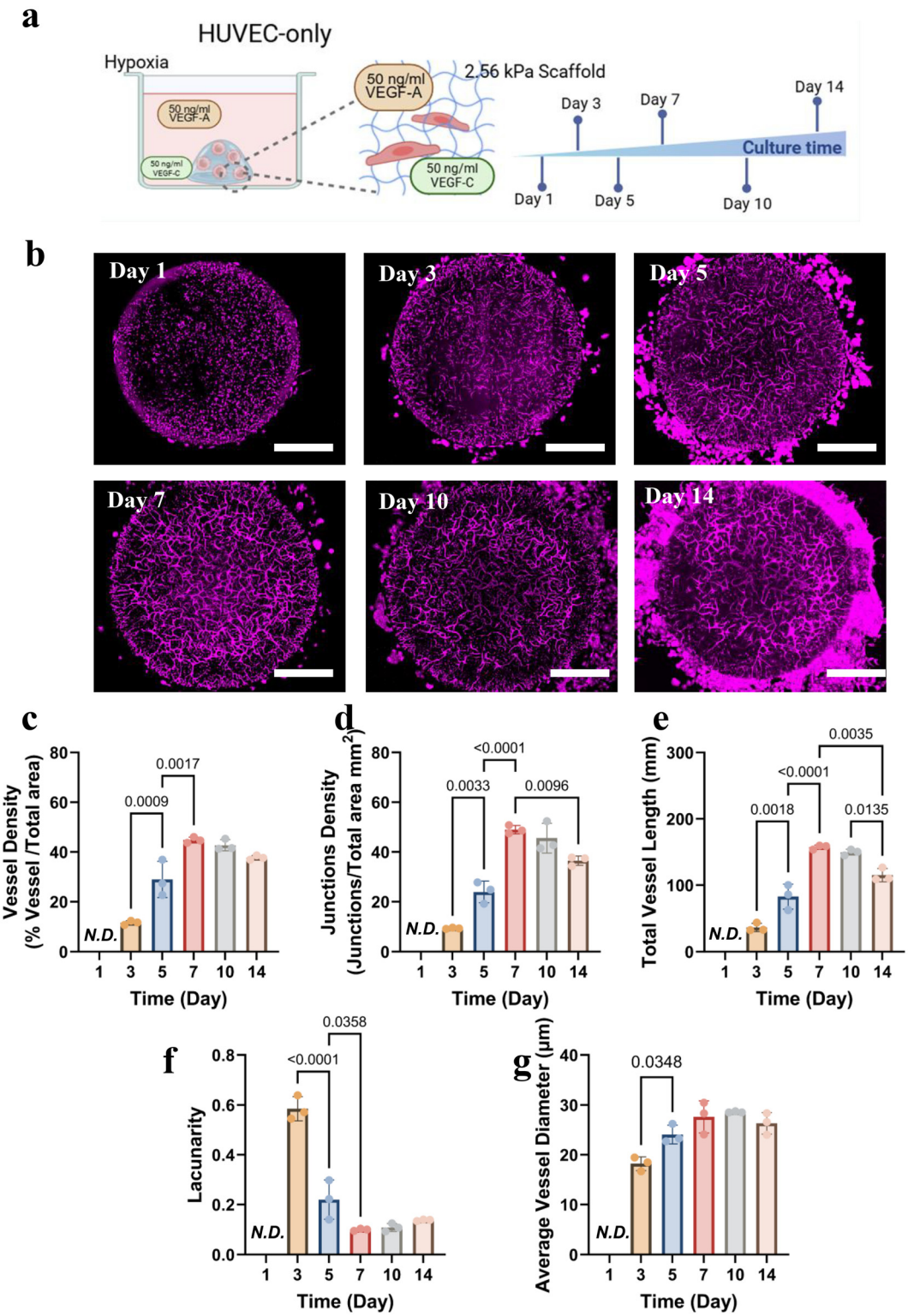

Fig. 4 Optimization of culture time for HUVEC-only capillary networks. (a) Schematic representation. (b) Observation of blood capillary by CD31 immunostaining under CLSM. Culture HUVEC-only tissue (2×10^4 HUVEC) in hypoxia (1% O_2) on a 2.56 kPa fibrin scaffold for 1, 3, 5, 7, 10, and 14 days. Scale bar = 1 mm. (c–g) The vessel density, total vessel length, junction density, lacunarity, and average vessel diameter in the whole microtissue of the 3D capillary structure were calculated by AngioTool (n = 3). Statistical analysis was performed using one-way ANOVA followed by Tukey's test. P-Values indicate significance. N.D. means not detected.

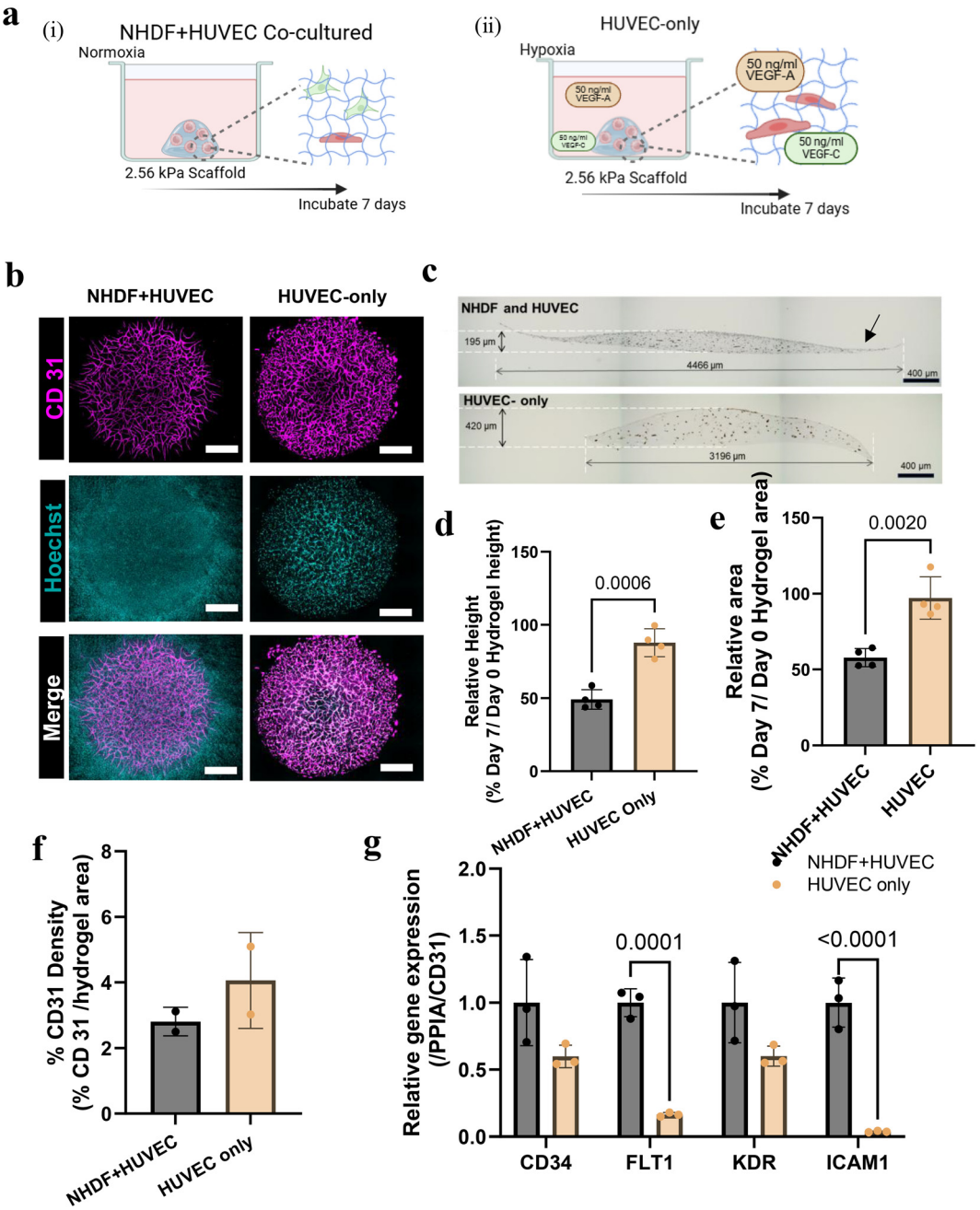

Fig. 5 Cells and vasculature localization and gene expression related to blood capillary. (a) Schematic illustration of the optimized experimental design. (b) CLSM images showing CD31 (pink) and Hoechst (blue) staining in the two capillary models. Scale bar 1 mm. (c) CD31 immunohistochemistry of both models. Scale bar 400 µm. White lines indicate hydrogel diameter and height. Black arrow shows NHDF cell layer. (d–f) Quantification of relative hydrogel height (d) (n = 4), diameter (e) (n = 4), and CD31 expression (f) (n = 2) after 7 days of culture. Statistical analysis in (d–f) was performed using a one-way t-test. (g) Gene expression analysis of vascular markers by qRT-PCR (n = 3). Statistical analysis by two-way ANOVA with Tukey's test. P-Values indicate significance.

we found that a matrix stiffness of 2.56 kPa combined with a seeding density of 30 000 cells enabled the formation of a stable and well-organized capillary network (Fig. S9). Based on this optimization, we further compared BMEC-only and BMEC + HA + HP co-cultures under both normoxic and hypoxic conditions using the selected parameters (2.56 kPa, 3 × 10^4 BMECs) (Fig. 6a). As a positive control, the BMEC co-culture under normoxia generated capillary networks with a total vessel length of 154.0 mm, slightly exceeding that observed under hypoxia (129.4 mm). Interestingly, the BMEC-only group under hypoxic conditions formed capillary networks with a total length of 159.7 mm, which was not statistically different from the BMEC co-culture under normoxia (Fig. 6b).

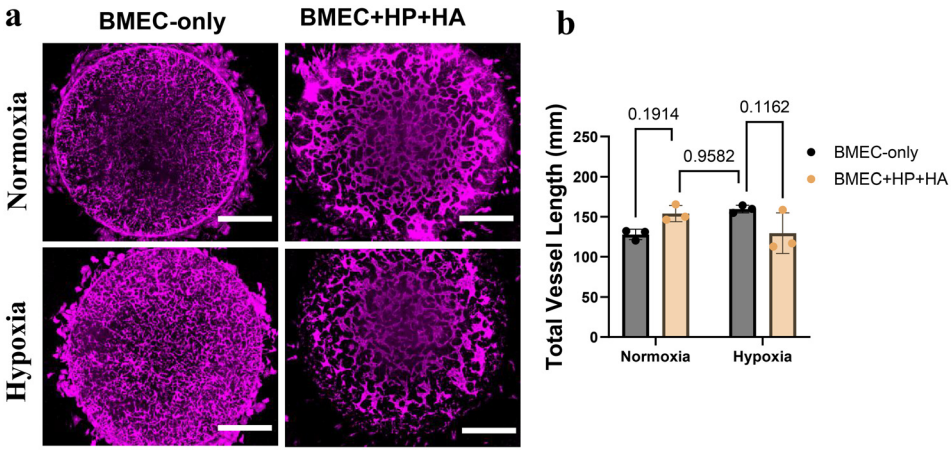

Fig. 6 Construction of monocultured blood capillary networks using other endothelial cell lines. (a) Observation of blood capillary by CD31 immunostaining under CLSM. Culture BMECs-only tissue (3×10^4 BMECs) in both normoxia (21% O_2) and hypoxia (1% O_2) on a 2.56 kPa fibrin scaffold for 7 days. Co-cultured group contains BMECs (3×10^4), HA (6×10^4), and HP (1.5×10^4) are cultured in the same environment as a positive control. Scale bar = 1 mm. (b) The total vessel length in the whole microtissue of the 3D capillary structure was calculated by AngioTool (n = 3). Statistical analysis was performed using one-way ANOVA followed by Tukey's test. P-Values are indicated directly on the graph to denote statistical significance.

In contrast, SECs were able to form capillary-like networks at a lower seeding density (0.5×10^4 cells) when embedded in a softer matrix (0.45 kPa) (Fig. S10). However, the resulting vessel diameters were larger than those observed in the positive control group composed of SECs co-cultured with LX-2 (Fig. S11).

4. Discussion

Hypoxia appeared as one of the key factors in angiogenesis, involving the activation of local cells to produce pro-angiogenic factors such as VEGF and cytokines. The initiation of the angiogenic program is preceded by the activation of EC which were in a quiescent state by biochemical signals such as VEGF. Under normoxia (21% O_2), in monoculture systems, increasing EC density often led to abnormal capillary network formation, characterized by enlarged, fused lumens. This phenomenon is not limited to HUVECs, induced pluripotent stem cell-derived endothelial cells (iPSC-ECs), used to construct brain microvascular networks in the presence of 50 ng mL^{-1} exogenous VEGF-A, also exhibited aberrant vascular fusion.[10] This may result from the excessive stimulation of VEGF receptors by exogenous VEGF, bypassing intrinsic regulatory mechanisms and disrupting the controlled progression of angiogenesis.[21,22]

In contrast, under hypoxic conditions (1% O_2), cells engage in the regulation of multiple signaling pathways that upregulate endogenous VEGF expression. VEGF activity under hypoxia is tightly regulated to ensure proper control of vessel diameter. The BMEC-only group consistently showed smaller lumens under both normoxic and hypoxic conditions. This may be due to the limited capacity of BMECs to undergo vascular fusion and form large-diameter vessels, even when exposed to elevated VEGF levels. As a result, BMECs tend to produce vascular networks with lower vessel density.

Although hypoxia is known to induce VEGF transcription and promote vascular development, it cannot fully substitute for exogenous VEGF supplementation (Fig. S3). Oladipupo *et al.* found that, in the absence of VEGF, hypoxia promoted the up-regulation of pro-angiogenesis related targets such as PIGF and Ang 2 but failed to produce new blood vessels.[23] In co-culture models, hypoxia led to a reduction in both vessel density and total vessel length, potentially due to fibroblast dysfunction caused by prolonged low oxygen. This may impair fibroblast migration, proliferation, and growth factor secretion, ultimately limiting angiogenesis.[5]

At the cellular level, sprouting angiogenesis begins when ECs escape the existing vessel wall, enzymatically degrade the basement membrane, change morphology, proliferate, and invade surrounding tissue while maintaining vascular continuity.[24] Tip cells at the leading edge of the sprout are highly migratory and responsive to environmental cues, whereas trailing stalk cells proliferate to extend the vessel. A balanced growth rate between these two cell populations is critical for the formation of stable capillary sprouts.[25] In soft hydrogels (0.45–0.71 kPa), ECs migrate rapidly, leading to the formation of thin, filamentous capillary structures in both monoculture and co-culture models. However, this rapid migration may outpace stalk cell proliferation, resulting in unstable or immature sprouts.[20,25,26] In contrast, stiffer hydrogels (2–15 kPa) restore the balance between tip cell migration and stalk cell proliferation, promoting the formation of stable, larger-diameter capillaries. Nevertheless, high fibrin density can hinder cell migration, communication, and nutrient transport.[27,28] Intermediate stiffness (~2.56 kPa) appears to support optimal vascular growth and stabilization.

Interestingly, when NHDFs or other support cells such as pericytes are incorporated into the hydrogel, angiogenesis becomes more responsive to the matrix environment due to paracrine and juxtacrine signaling. These support cells secrete pro-angiogenic factors such as VEGF and bFGF-2 in close proximity to ECs, adopt pericyte-like phenotypes, and facilitate vascular maturation while protecting ECs from apoptosis.[29,30] As a result, co-cultured systems display greater adaptability to changes in matrix stiffness and composition, leading to more robust and stable vessel formation. However, it should be emphasized that the optimal stiffness is highly dependent on both the endothelial cell type and the choice of matrix material.[31] For instance, SECs exhibited maximal vascular growth at ~0.56 kPa (Fig. S10), whereas BMECs, similar to HUVECs, displayed more robust vascularization at ~2.56 kPa (Fig. S9). In studies employing HUVECs as the endothelial source, Lu *et al.* reported that intermediate-stiffness silk fibroin (SF) scaffolds (3–7.4 kPa) supported the most favorable vascular network formation.[32] By contrast, Schweller *et al.* demonstrated in PEGDA hydrogels around 1–17 kPa that softer matrices (~1 kPa) were most permissive for vascular growth.[33] Together, these findings highlight that "optimal" stiffness is not universally fixed but depends critically on the interplay between cell type and matrix composition. Nevertheless, it is widely recognized that relatively soft matrices are generally more conducive to vascular growth.

Lacunarity is a measure used to describe the size distribution of gaps or voids surrounding objects within an image. Higher lacunarity values indicate a broader distribution of gap sizes, corresponding to a greater degree of irregularity or heterogeneity in the spatial pattern.[34,35] However, no significant differences in lacunarity were observed between different VEGF concentrations or types (Fig. S12), suggesting that spatial heterogeneity of the vascular networks was not strongly influenced by VEGF in this context. Similarly, lacunarity values did not differ markedly between the co-culture and monoculture models in softer matrices (0.45–2.56 kPa). In contrast, for matrices with stiffness above 5 kPa, both models exhibited a pronounced increase in heterogeneity (Fig. S13). Matrix remodeling and endothelial development during angiogenesis inevitably lead to fibrin degradation. Histological analysis clearly shows that the gel volume in the co-culture group decreased significantly, indicating a faster degradation rate compared to the monoculture group.

Following endothelial sprouting, vessel structures undergo cytoplasmic fusion and stabilize through the influence of growth factors or supporting cells. Prolonged hypoxia (>48 h) enhances VEGFR1-mediated intracellular signaling in response to exogenous VEGF-A, triggering a negative feedback loop that promotes vascular stabilization.[36] VEGF-C not only activates VEGFR2 to drive endothelial cell proliferation and migration, but also stimulates VEGFR3, facilitating stabilization at vessel fusion sites.[37] However, due to potential saturation of VEGF receptors, exogenous VEGF-A and VEGF-C alone may be insufficient to replicate the robust vascular maturation effects provided by NHDFs, which secrete a broad range of pro-angiogenic factors including FGF, PDGF, and VEGF.[38] This likely explains the slight degradation observed in monoculture capillary networks after 10 days, as VEGF alone lacks the capacity to maintain mature vessels.[39] Furthermore, while FGF-2, VEGF-A, and VEGF-C all promote angiogenesis, their efficacy differs (VEGF-A < VEGF-C < FGF-2).[40]

Finally, at 7 days of culture, despite the lower expression found for the key angiogenic and endothelial activation markers observed in HUVEC-only monocultures compared to HUVEC + NHDF co-cultures, these findings do not necessarily indicate inferior vasculature maturation. Rather, they may reflect a more quiescent and stabilized endothelial phenotype, consistent with the absence of scaffold degradation observed. In the absence of NHDF secreted paracrine factors, HUVECs may actually downregulate genes involved in active sprouting and proliferation. Both, ICAM-1 and VEGFR-2 (KDR) are generally upregulated in activated endothelium during angiogenesis or inflammation, being a hallmark of active endothelial proliferation and vessel sprouting,[13,41] and their reduced expression in HUVEC-only cultures may only reflect a transition toward a more mature, less angiogenically active state. Importantly, the balance between pro- and anti-angiogenic signaling is essential for proper vascular development and homeostasis. Excessive VEGF signaling can result in "abnormal" vascular features, such as excessive vessel dilation and increased permeability.[42] Hence, endogenous regulatory mechanisms may downregulate VEGFR expression to mitigate these effects, facilitating vessel pruning and remodeling toward a more physiologically stable vascular architecture.[13,43]

In summary, our findings suggest that optimal capillary growth occurs at a matrix stiffness of ~2.56 kPa and VEGF concentrations above 50 ng ml^{-1}, reflecting a balance between mechanical support and biochemical stimulation (Fig. S16). These parameters could serve as the basis for developing scaling relationships that link sprouting dynamics, incorporating traction forces, chemotactic signaling, and matrix remodeling, providing a foundation for future physics-informed and computational models of capillary morphogenesis.

5. Conclusion

We successfully established a capillary network model using only human endothelial cells under hypoxia by tuning both growth factors (VEGF-A and VEGF-C) and hydrogel stiffness. Taken together, these findings suggest that HUVEC-only vascularization may offer distinct advantages in engineered tissues where structural predictability and matrix preservation are critical. This monoculture model can form vessels without relying on stromal cell-mediated junction regulation, making it possible to promote vascular growth solely through the addition of essential cytokines. Also, it avoids potential stromal cell–induced disruption and can be integrated into other organotypic models to advance organoid engineering. Moreover, we have confirmed that this monoculture approach can successfully generate capillary-like structures using brain

microvascular endothelial cell lines (BMEC) or liver endothelial cell lines (SEC), providing a foundation for its broad applicability.

Author contributions

He Li: writing – original draft, methodology, investigation, formal analysis, data curation, conceptualization. Fiona Louis: writing – review & editing, validation, methodology, conceptualization. Michiya Matsusaki: writing – review & editing, supervision, conceptualization funding acquisition.

Conflicts of interest

There are no conflicts to declare.

Abbreviations

VEGF	Vascular endothelial growth factor
BMEC	Brain microvascular endothelial cells
SEC	Liver sinusoidal endothelial cells
ECs	Endothelial cells
FGF	Fibroblast growth factor
PDGF	Platelet-derived growth factor
TGF-β	Transforming growth factor-beta
MMP	Matrix metalloproteinases
HIF	Hypoxia-inducible factor
PlGF	Placental growth factor
ANG-1	Angiopoietin-1
ANG-2	Angiopoietin-2
PAI-1	Plasminogen activator inhibitor-1
ECM	Extracellular matrix
NHDF	Normal human dermal fibroblast cells
LX-2	Cryopreserved human hepatic stellate cells
HP	Human brain vascular pericytes
HA	Human astrocytes
HE	Hematoxylin eosin
iPSC-ECs	Pluripotent stem cell-derived endothelial cells
IHC	Immunohistochemistry

Data availability

The data supporting this article have been included as part of the supplementary information (SI). Supplementary information is available. See DOI: https://doi.org/10.1039/d5bm00981b.

Acknowledgements

This study was financially supported by KAKENHI JP22H05131, JP22H05138, JP22H05140, JP22H05141, JP25H01220, JP22K21348, and JP21H04634 from Japan Society for Promotion of Science (JSPS). This study was also supported by JPJSBP120239201, JPJSBP120252301, and Y2024L0906033 from JSPS, COI-NEXT (JPMJPF2009) from Japan Science and Technology Agency (JST), and JPNP231053211 and JPNP21502154-0 commissioned by the New Energy and Industrial Technology Development Organization (NEDO).

References

1 J. P. Morgan, P. F. Delnero, Y. Zheng, S. S. Verbridge, J. Chen, M. Craven, N. W. Choi, A. Diaz-Santana, P. Kermani, B. Hempstead, J. A. López, T. N. Corso, C. Fischbach and A. D. Stroock, *Nat. Protoc.*, 2013, **8**, 1820.
2 C. J. Kirkpatrick, S. Fuchs and R. E. Unger, *Adv. Drug Delivery Rev.*, 2011, **63**, 291.
3 C. Hausmann, C. Zoschke, C. Wolff, M. E. Darvin, M. Sochorová, A. Kováčik, B. Wanjiku, F. Schumacher, J. Tigges, B. Kleuser, J. Lademann, E. Fritsche, K. Vávrová, N. Ma and M. Schäfer-Korting, *Sci. Rep.*, 2019, **9**, 2913.
4 P.-S. Chen, W.-T. Chiu, P.-L. Hsu, S.-C. Lin, I.-C. Peng, C.-Y. Wang and S.-J. Tsai, *J. Biomed. Sci.*, 2020, **27**, 63.
5 M. Oberringer, C. Meins, M. Bubel and T. Pohlemann, *Biol. Cell*, 2007, **99**, 197–207.
6 E. Kniazeva, S. Kachgal and A. J. Putnam, *Tissue Eng., Part A*, 2011, **17**, 905.
7 Y. Tan, M. Zhang, Y. Kong, F. Zhang, Y. Wang, Y. Huang, W. Song, Z. Li, L. Hou, L. Liang, X. Guo, Q. Liu, Y. Feng, C. Zhang, X. Fu and S. Huang, *Bioeng. Transl. Med.*, 2024, **9**, e10630.
8 S. Y. Yoo and S. M. Kwon, *Mediators Inflammation*, 2013, **2013**, 127170.
9 T. Fujita, T. Yuki and M. Honda, *Regen. Ther.*, 2024, **25**, 138.
10 M. Campisi, Y. Shin, T. Osaki, C. Hajal, V. Chiono and R. D. Kamm, *Biomaterials*, 2018, **180**, 117.
11 Y. B. Li, C. Sodja, M. Rukhlova, J. Nhan, J. J. A. Poole, H. Allen, S. Yimer, E. Baumann, E. Bedford, H. Prazak, W. J. Costain, S. Murugkar, J.-P. St-Pierre, L. Mostaço-Guidolin and A. Jezierski, *Bioprinting*, 2023, **30**, e00258.
12 H. Li, Y. Shang, J. Zeng and M. Matsusaki, *Nano Converg.*, 2024, **11**, 10.
13 M. Shibuya, *Genes Cancer*, 2011, **2**, 1097.
14 T. Tammela, G. Zarkada, E. Wallgard, A. Murtomäki, S. Suchting, M. Wirzenius, M. Waltari, M. Hellström, T. Schomber, R. Peltonen, C. Freitas, A. Duarte, H. Isoniemi, P. Laakkonen, G. Christofori, S. Ylä-Herttuala, M. Shibuya, B. Pytowski, A. Eichmann, C. Betsholtz and K. Alitalo, *Nature*, 2008, **454**, 656.
15 B. L. Krock, N. Skuli and M. C. Simon, *Genes Cancer*, 2011, **2**, 1117.
16 R. G. M. Breuls, T. U. Jiya and T. H. Smit, *Open Orthop. J.*, 2008, **2**, 103.
17 M. A. Abdul Sisak, F. Louis, S. Hyeok Lee, Y.-T. Chang and M. Matsusaki, *Micromachines*, 2020, **11**, 727.
18 E. Zudaire, L. Gambardella, C. Kurcz and S. Vermeren, *PLoS One*, 2011, **6**, e27385.

19 K. O. Rojek, A. Wrzos, S. Żukowski, M. Bogdan, M. Lisicki, P. Szymczak and J. Guzowski, *APL Bioeng.*, 2024, **8**, 016106.
20 H. Duong, B. Wu and B. Tawil, *Tissue Eng., Part A*, 2009, **15**, 1865.
21 C. J. Drake and C. D. Little, *Proc. Natl. Acad. Sci. U. S. A.*, 1995, **92**, 7657.
22 C. J. Drake and C. D. Little, *J. Histochem. Cytochem.*, 1999, **47**, 1351.
23 S. Oladipupo, S. Hu, J. Kovalski, J. Yao, A. Santeford, R. E. Sohn, R. Shohet, K. Maslov, L. V. Wang and J. M. Arbeit, *Proc. Natl. Acad. Sci. U. S. A.*, 2011, **108**, 13264.
24 R. Blanco and H. Gerhardt, *Cold Spring Harbor Perspect. Med.*, 2013, **3**, a006569.
25 A. Shamloo and S. C. Heilshorn, *Lab Chip*, 2010, **10**, 3061.
26 C. Coulon, M. Georgiadou, C. Roncal, K. De Bock, T. Langenberg and P. Carmeliet, *Arterioscler. Thromb. Vasc. Biol.*, 2010, **30**, 2331.
27 D. Gomez, S. Natan, Y. Shokef and A. Lesman, *Adv. Biosyst.*, 2019, **3**, 1900192.
28 K. Liu, M. Wiendels, H. Yuan, C. Ruan and P. H. J. Kouwer, *Bioact. Mater.*, 2022, **9**, 316.
29 C. M. Ghajar, S. Kachgal, E. Kniazeva, H. Mori, S. V. Costes, S. C. George and A. J. Putnam, *Exp. Cell Res.*, 2010, **316**, 813.
30 L. Lamalice, F Le Boeuf and J. Huot, *Circ. Res.*, 2007, **100**, 78.
31 Y. Wang, M. Liu, W. Zhang, H. Liu, F. Jin, S. Mao, C. Han and X. Wang, *Burns Trauma*, 2024, **12**, tkae039.
32 X. Lu, Z. Ding, F. Xu, Q. Lu and D. L. Kaplan, *ACS Appl. Bio Mater.*, 2019, **2**, 3108.
33 R. M. Schweller and J. L. West, *ACS Biomater. Sci. Eng.*, 2015, **1**, 335.
34 D. J. Gould, T. J. Vadakkan, R. A. Poché and M. E. Dickinson, *Microcirculation*, 2011, **18**, 136.
35 D. Guidolin, B. Nico, G. Mazzocchi, A. Vacca, G. G. Nussdorfer and D. Ribatti, *Leukemia*, 2004, **18**, 1745.
36 C. Ulyatt, J. Walker and S. Ponnambalam, *Biochem. Biophys. Res. Commun.*, 2011, **404**, 774.
37 J.-L. Thomas, K. Baker, J. Han, C. Calvo, H. Nurmi, A. C. Eichmann and K. Alitalo, *Cell. Mol. Life Sci.*, 2013, **70**, 1779.
38 R. K. Jain, *Nat. Med.*, 2003, **9**, 685.
39 G. D. Yancopoulos, S. Davis, N. W. Gale, J. S. Rudge, S. J. Wiegand and J. Holash, *Nature*, 2000, **407**, 242.
40 R. Cao, A. Eriksson, H. Kubo, K. Alitalo, Y. Cao and J. Thyberg, *Circ. Res.*, 2004, **94**, 664–670.
41 W. Langston, J. H. Chidlow, B. A. Booth, S. C. Barlow, D. J. Lefer, R. P. Patel and C. G. Kevil, *Free Radicals Biol. Med.*, 2007, **42**, 720.
42 D. Fukumura and R. K. Jain, *Microvasc. Res.*, 2007, **74**, 72.
43 Z. Zhang, K. G. Neiva, M. W. Lingen, L. M. Ellis and J. E. Nör, *Cell Death Differ.*, 2010, **17**, 499.

